JOURNAL OF QUATERNARY SCIENCE (2013) **28**(5) 501–514 ISSN 0267-8179. DOI: 10.1002/jqs.2641

Cryptotephrochronology of the Eemian and the last interglacial–glacial transition in the North East Atlantic

PETER M. ABBOTT,[1]* WILLIAM E. N. AUSTIN,[2] SIWAN M. DAVIES,[1] NICHOLAS J. G. PEARCE[3] and FIONA D. HIBBERT[2†]

[1]Department of Geography, College of Science, Swansea University, Singleton Park, Swansea SA2 8PP, UK
[2]School of Geography and Geosciences, University of St Andrews, North Street, St Andrews, UK
[3]Institute of Geography and Earth Sciences, Aberystwyth University, Llandinam Building, Penglais Campus, Aberystwyth, UK

Received 18 January 2013; Revised 26 March 2013; Accepted 27 March 2013

ABSTRACT: The Eemian interglacial and the onset of the subsequent glacial period serve as the most recent analogue for the natural operation of the climate system during the current interglacial. Pronounced climatic oscillations occurred during this period, but their nature and pattern are poorly understood due to dating limitations and unknown phase relationships between different regions and archives. Tephrochronology offers considerable potential for precise correlation of disparate palaeoclimatic archives preserving evidence of these rapid climatic transitions through the tracing of common isochronous tephra horizons. We outline the identification of three previously unknown cryptotephra horizons within a marine core from the Rockall Trough, North East Atlantic. This sequence preserves a high-resolution record of this interval and shard size, geochemical heterogeneity and the covariance of shard concentrations with ice-rafted debris data are utilized to demonstrate that primary airfall was the most likely transport and depositional pathway. The main geochemical populations of these horizons have similar transitional alkali major and trace element compositions, suggesting that they were derived from a common Icelandic source, potentially the Öræfajökull volcanic system. These tephra horizons represent additions to the North Atlantic event stratigraphy for this period and tentative correlations to Icelandic terrestrial deposits are proposed for two horizons. Copyright © 2013 John Wiley & Sons, Ltd.

KEYWORDS: cryptotephra; Iceland; isochrons; palaeoclimatic correlation; volcanic ash.

Introduction

Termination II, the Eemian and the last interglacial–glacial transition

Marine isotope stages (MIS) 6–4 encompasses the deglaciation that occurred at the end of MIS 6 (i.e. Termination II), the last interglacial period (i.e. the Eemian or MIS 5e), the penultimate glacial inception period (i.e. MIS 5) and the transition to major global cooling (i.e. MIS 4). MIS 5e is the most recent interglacial and a fuller understanding of climate dynamics during this interval may aid the understanding of natural climatic mechanisms during warm periods. In addition, there is increasing evidence that millennial- to centennial-scale, abrupt and pronounced climate oscillations occurred throughout MIS 6– 4 in the North Atlantic region during periods characterized by changing climatic boundary conditions (e.g. McManus *et al.*, 1994, 1999, 2002; Lototskaya and Ganssen, 1999; Oppo *et al.*, 2001; Knudsen *et al.*, 2002; North Greenland Ice Core Project Members, 2004; Capron *et al.*, 2010). Determining the regional response to these climatic changes is crucial to improving the understanding of the forcing mechanisms controlling these abrupt events, and central to this is high-precision correlation and synchronization of the disparate palaeoclimatic archives.

Tephrochronology is a powerful technique that can be used to achieve these goals, especially for sequences that extend beyond ~50 ka as they fall outside the radiocarbon dating window. Previous tephrostratigraphical investigations of this period have identified numerous horizons within North Atlantic marine sequences (e.g. from the Faroe Islands region, the Norwegian Sea and the area north of Iceland; Fronval *et al.*, 1998; Lacasse *et al.*, 1998; Wastegård and Rasmussen, 2001; Brendryen *et al.*, 2010) and within both the NGRIP and GRIP ice-core records (Grönvold *et al.*, 1995; Abbott *et al.*, 2012) (Fig. 1). Here we build on work by Abbott *et al.* (2011) on a marine record from the Rockall Trough and add to the existing tephrostratigraphical framework for Greenland and the North Atlantic region. This investigation utilizes a range of data sources, such as high-resolution ice-rafted debris (IRD) flux, to assess the transport and secondary depositional history of tephra horizons, an essential first step if marine horizons are to be used as isochronous tie-lines [see discussions in Austin *et al.* (2004), Brendryen *et al.* (2010) and Abbott *et al.* (2011)].

Tephrochronology is one of a range of event stratigraphy techniques available for the construction of chronological models for marine sequences. Beyond the radiocarbon window several methods are available, including the definition of local event-stratigraphies (e.g. Austin *et al.*, 2012), tuning of isotopic records to regional stratotypes, such as the NGRIP ice-core, or global isotopic stacks, such as the LR04 stack of Lisiecki and Raymo (2005), and magnetostratigraphy (see Austin and Hibbert, 2012). If they can be traced, tephra horizons add exceptional value to chronological models developed in this way by providing isochronous tie-lines between sequences that independently validate correlations between records and help to overcome some of the problems inherent to the other techniques (see Austin and Hibbert, 2012). An essential first step for this work, however, is to establish a detailed framework of volcanic events that can be exploited in this way.

MD04-2822 and the last interglacial–glacial transition

The 37.7-m-long MD04-2822 core was retrieved from the deep-water margins of the Barra Fan in the Rockall Trough

*Correspondence: P. M. Abbott, as above.
E-mail: p.abbott@swansea.ac.uk
†Present address: Ocean and Earth Sciences, University of Southampton, National Oceanography Centre, Southampton SO14 3ZH, UK

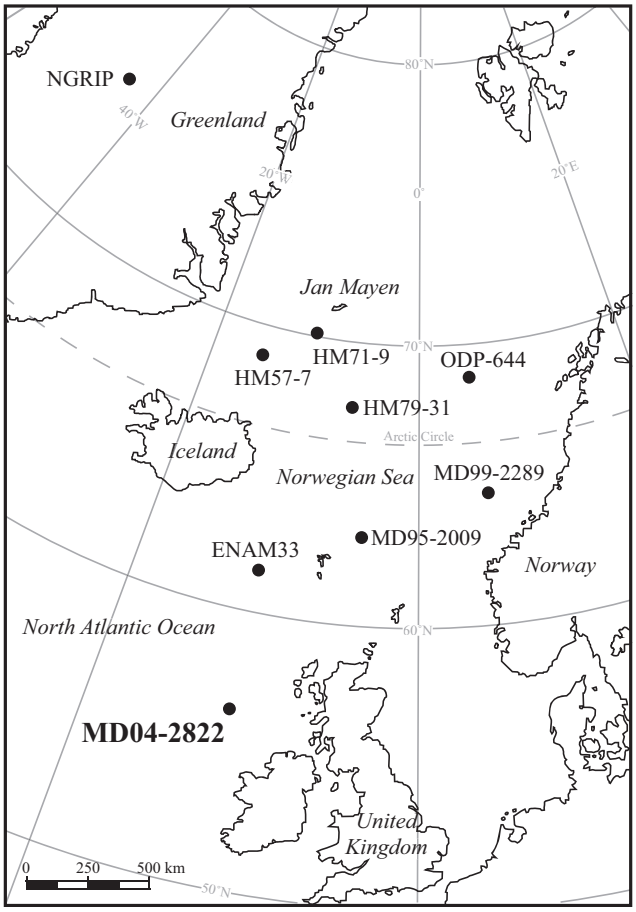

Figure 1. Location map of the drilling sites for MD04-2822 and other North Atlantic cores preserving MIS 6–4 tephra horizons.

area during 2004 (Fig. 1; 56°50.54′N, 11°22.96′W). The penultimate glaciation (MIS 6), last interglacial (LIG; MIS 5e) and glacial inception are clearly evident within the benthic $\delta^{18}O$ record of MD04-2822 (Fig. 2iii). Co-registered surface proxies [% abundance of *Neogloboquadrina pachyderma* (sinistral)] indicate a rapid movement of the polar front northwards during Termination II, with generally clement surface conditions throughout MIS 5 and the LIG coinciding with low IRD flux to the site (Fig. 2). Punctuations of cooler conditions and enhanced IRD delivery are, however, evident through MIS 5, consistent with the pan-Atlantic 'C-events' (e.g. McManus *et al.*, 1994; Chapman and Shackleton, 1999), which are thought to relate to the Dansgaard–Oeschger events recorded in the Greenland ice-cores (Rousseau *et al.*, 2006). The polar front migrates southward once more at the start of MIS 4 and IRD flux to the site becomes a persistent feature of the record and its provenance suggests a renewed contribution from an expanding British and Irish Ice Sheet (BIIS) with calving margins on the adjacent Hebridean shelf at this time (Hibbert *et al.*, 2010; Fig. 2).

Within MD04-2822, Termination II, the last interglacial and the last interglacial–glacial transition occur between 2200 and 2700 cm depth and the tephrostratigraphy of the top part of this section (2200–2380 cm) was outlined in Abbott *et al.* (2011). This study builds on the previous investigation, which demonstrated the successful application of density separation and trace element analysis techniques within the investigation of marine tephra horizons. Two tephra horizons of MIS 4 age, thought to be derived from primary airfall, were identified within the fine fraction of the sediments. Here we utilize the same techniques over the MIS 5 period for MD04-2822 to identify tephra horizons that may, in the future, help synchronize this record to the NGRIP ice-core. This offers the potential to resolve chronological differences and uncertainties in timing between Greenland ice-core records and North Atlantic marine records.

Icelandic volcanic history

Geochemical characterization of both the major and the trace element composition of tephra horizons permits robust correlation of tephra horizons between disparate sequences and helps pinpoint the likely source volcanic regions. Iceland is the primary source of tephra in North Atlantic marine records and recent tephrostratigraphical investigations of the

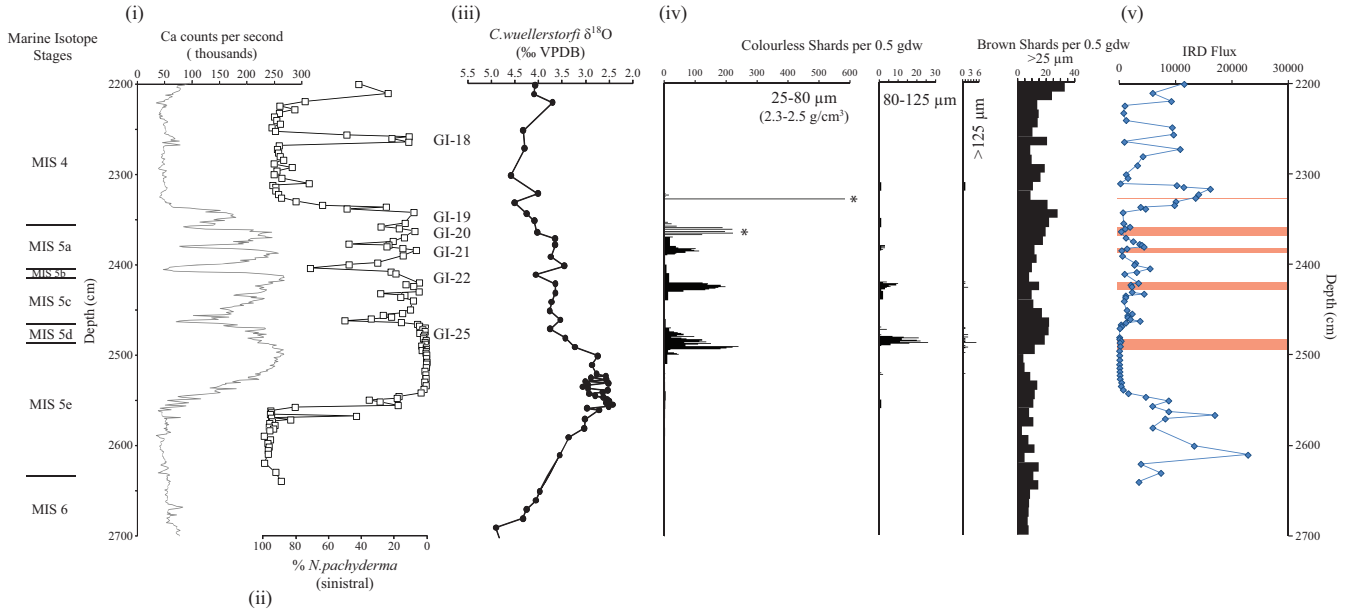

Figure 2. Climatic and tephra stratigraphy of the MIS 4–6 period within MD04-2822. (i) XRF (ITRAX core scanning) Ca count rates, (ii) high-resolution percentage abundance of *Neogloboquadrina pachyderma* (*sinistral*), (iii) *Cibicidoides wuellerstorfi* $\delta^{18}O$ record, (iv) tephrostratigraphy incorporating 10-cm and 1-cm resolution shards counts. The high-resolution colourless shard counts from 2200 to 2380 cm depth and horizons marked with * are described in Abbott *et al.* (2011). (v) High-resolution IRD flux. Red bars denote sections with high tephra shard concentrations. This figure is available in colour online at wileyonlinelibrary.com.

MIS 6 to 4 period highlights that our knowledge of the Icelandic volcanic history is still far from complete (Abbott *et al.*, 2011, 2012). Furthermore, recent Ar–Ar dating of terrestrial deposits in Iceland suggests that a number of rhyolitic eruptions occurred during this time (e.g. McGarvie *et al.*, 2006, 2007; Flude *et al.*, 2010). The identification of these deposits in marine sequences has the potential to provide more precise stratigraphic and chronological constraints on these volcanic events than can be achieved solely from proximal Icelandic sequences. This has the potential to improve our understanding of the repose periods for specific volcanic systems, allow us to determine whether volcanic systems have geochemically evolved over time and explore the possibility that volcanism might be climatically driven by changes in crustal stresses (Flude *et al.*, 2010).

Materials and methods

Quantification of tephra content and shard size distribution

The tephra content of the core sequence between 2380 and 2700 cm depth was initially investigated at a 10-cm contiguous resolution. Intervals of higher shard concentration displaying a distinct peak relative to background levels in this record were subsequently analysed at a 1-cm resolution to refine the stratigraphic position of any peaks in tephra concentration. All samples were prepared using a procedure modified from those outlined in Turney (1998), Davies *et al.* (2005) and Blockley *et al.* (2005). Sediment samples were freeze-dried and 0.5 g of dry weight sediment (gdw) from each sample was prepared. Carbonate material was removed from the samples through immersion in dilute (10%) hydrochloric acid (HCl) overnight. The sediment was separated into three grain size fractions (>125, 80–125 and 25–80 μm diameters) using 125- and 80-μm wire mesh sieves and 25-μm nylon sieve mesh. The 25–80 μm grain size fraction was further isolated into three density fractions (<2.3, 2.3–2.5 and >2.5 g cm^{-3}) using the heavy liquid sodium polytungstate [$Na_6(H_2W_{12}O_{40})H_2O$]. The >125 and 80–125 μm grain size fractions and the 2.3–2.5 and >2.5 g cm^{-3} density fractions of the 25–80-μm material were mounted on microscope slides in Canada Balsam before optical microscopy was used to identify glass tephra shards.

The size distribution of material within shard concentration peaks was determined by measuring the long axis diameter of 100 randomly selected individual shards from the samples chosen for geochemical analysis. To ensure this analysis was representative, for each peak the proportion of shards measured from each grain size fraction was consistent with the proportion of that grain size within the total shard count for the peak, i.e. 85 shards from the 25–80 μm fraction were measured if 85% of the total number of shards counted were from that size fraction.

Age assignment for tephra horizons

The chronology for the core was described by Hibbert *et al.* (2010) but has recently been updated using the GICC05 time scale (GICC05modelext. time scale; see Svensson *et al.*, 2008; Wolff *et al.*, 2010 and references therein; see Austin and Hibbert, 2012). Age control was primarily achieved via the visual correlation of the abrupt warming in the percentage *N. pachyderma* (sinistral) record to the NGRIP $\delta^{18}O$ record (North Greenland Ice Core Project Members, 2004) with additional tie-points deriving from the correlation of the benthic $\delta^{18}O$ to the LR04 stack (Lisiecki and Raymo, 2005). Within the MD04-2822 age model, age uncertainties associated with each tie-point include those associated with the ice core/benthic $\delta^{18}O$ stack (i.e. ice core/LR04 age uncertainty), the process of tuning (e.g. the potential error in determining the position of the tie-point within the MD04-2822 record, sample spacing, etc.) and the likely bioturbation extent of the sediments. We have propagated the uncertainties for each tie-point using a mean squared estimate from which we have been able to estimate the minimum uncertainty associated with the inferred age for the identified tephra horizons. This chronology allows ages with associated uncertainties to be assigned to the identified tephra horizons within the record.

Geochemical characterization of tephra shards

Material selected for geochemical analysis was prepared using the methodology outlined above, except that the material was mounted on 28 × 48-mm microscope slides in epoxy resin to permit the creation of thin sections of individual shards using silicon carbide paper and 6- and 1-μm diamond suspension solution.

The major element composition of individual shards was analysed using wavelength-dispersive electron-probe microanalysis (WDS EPMA) at the NERC Tephrochronological Analytical Unit at the University of Edinburgh. A Cameca SX100 electron microprobe with five vertical wavelength-dispersive spectrometers was used to gain oxide values for 13 major and minor elements. The operating conditions that were utilized are described in Hayward (2012) and further details are given in Table 1. Pure metals, synthetic oxides and silicate standards were used for calibration. The secondary standards of Cannetto Lami Lava, Lipari and BHVO-2g were analysed at regular intervals during the analytical period to monitor for drift and to assess the precision and accuracy of the glass analyses. Tables S1 and S2 in the online Supporting information report these analyses and highlight the close correspondence between these readings and reference values. Analyses were normalized to an anhydrous basis (i.e. 100% total oxides) for data comparison. Raw data values for the analyses are provided in supporting Tables S4–S6.

The trace element composition of individual shards was analysed at the Institute for Geography and Earth Sciences, Aberystwyth University, using laser ablation inductively coupled plasma mass spectrometry (LA-ICP-MS). The system employed couples a Coherent GeoLas 193-nm Excimer laser with a Thermo Finnigan Element 2 high-resolution sector field mass spectrometer (Pearce *et al.*, 2007, 2011). Operating conditions are outlined in Table 1. To calculate trace element concentrations, the methods outlined in Perkins and Pearce (1995) and Pearce *et al.* (2007) were used, with ^{29}Si acting as the internal standard and the NIST SRM 612 silicate glass as the calibration standard, with concentrations from Pearce *et al.* (1997). For glass analyses conducted at high spatial resolutions (using ablation craters 20 μm in diameter), there is a systematic bias between determined and accepted concentrations due to fractionation effects. To correct for this, a correction factor is applied to all analyses (see Pearce *et al.*, 2011 for further details). Corrected analyses of the USGS secondary standards BCR-2G and BHVO-2G conducted during the analytical period have a close match to reference values (supporting Table S3) and demonstrate the high accuracy of the LA-ICP-MS analyses reported in this study.

Treatment of geochemical outliers

Within most tephrochronological studies geochemical outliers can be dismissed as analytical anomalies, however, within marine tephra studies geochemical heterogeneity can be an important indicator of transport and/or depositional

Table 1. Mean (1σ standard deviation) major, minor and trace element values for the main populations within the three tephra deposits.

	MD04-2822		
	2385–2386 cm	2424–2425 cm	2490–2491 cm
Shards (*n*)	10	9	36
SiO_2	73.73 (0.30)	74.21 (0.48)	73.54 (0.44)
TiO_2	0.18 (0.01)	0.17 (0.02)	0.21 (0.02)
Al_2O_3	13.21 (0.15)	12.81 (0.06)	12.90 (0.17)
FeO	2.47 (0.10)	2.37 (0.28)	2.78 (0.21)
MnO	0.08 (0.01)	0.08 (0.01)	0.09 (0.01)
MgO	0.09 (0.01)	0.05 (0.02)	0.06 (0.02)
CaO	0.86 (0.11)	0.72 (0.07)	0.79 (0.07)
Na_2O	5.01 (0.12)	4.97 (0.13)	5.07 (0.15)
K_2O	3.92 (0.10)	4.08 (0.09)	4.02 (0.15)
P_2O_5	0.02 (0.01)	0.01 (0.01)	0.01 (0.01)
SO_2	0.00 (0.00)	0.01 (0.01)	0.01 (0.01)
F	0.19 (0.02)	0.25 (0.02)	0.26 (0.02)
Cl	0.23 (0.03)	0.28 (0.03)	0.25 (0.02)
Total oxides	95.49 (0.90)	95.89 (0.46)	95.43 (0.52)
Shards (*n*)	10	9	31
Rb (85)	92.04 (8.44)	94.99 (13.90)	98.38 (21.89)
Sr (88)	57.50 (22.24)	50.02 (10.03)	58.27 (14.72)
Y (89)	148.29 (18.23)	145.19 (13.35)	145.15 (25.35)
Zr (90)	619.41 (103.42)	646.13 (165.48)	807.88 (132.94)
Nb (93)	102.09 (17.03)	155.07 (21.99)	165.41 (11.74)
Cs (133)	1.32 (1.07)	1.20 (0.61)	1.29 (0.92)
Ba (138)	908.27 (122.16)	826.33 (108.30)	751.45 (106.12)
La (139)	115.64 (14.99)	136.47 (13.99)	132.81 (16.09)
Ce (140)	205.11 (26.09)	260.15 (23.05)	249.66 (25.17)
Pr (141)	26.72 (4.70)	31.16 (2.91)	30.89 (3.61)
Nd (143)	113.09 (13.20)	139.99 (22.07)	129.88 (19.41)
Sm (147)	24.32 (4.15)	25.31 (5.97)	24.47 (4.32)
Eu (151)	3.38 (1.16)	2.92 (0.94)	3.37 (1.09)
Gd (158)	22.16 (7.61)	26.76 (4.73)	27.08 (6.16)
Tb (159)	3.68 (0.76)	4.10 (1.20)	4.15 (0.90)
Dy (163)	28.81 (6.95)	29.14 (4.70)	27.98 (5.46)
Ho (165)	5.24 (1.08)	5.59 (1.11)	5.60 (1.04)
Er (166)	12.28 (2.52)	14.74 (3.85)	15.15 (3.52)
Tm (169)	2.30 (0.53)	2.15 (0.54)	2.09 (0.64)
Yb (174)	15.44 (2.79)	15.10 (3.28)	14.30 (2.93)
Lu (175)	1.53 (0.87)	1.98 (0.97)	1.87 (0.82)
Hf (178)	21.35 (6.25)	25.63 (6.22)	26.85 (5.41)
Ta (181)	8.25 (1.69)	11.30 (2.39)	11.80 (1.39)
Pb (208)	11.11 (1.26)	13.60 (3.85)	10.90 (2.37)
Th (232)	19.82 (3.80)	22.07 (2.64)	21.19 (3.43)
U (238)	4.51 (0.68)	4.84 (0.87)	4.96 (0.68)

Total oxide values are raw values before normalization. All major and minor elements are expressed as weight percentage. Trace elements expressed as p.p.m. Total iron is expressed as FeO. Numbers in parentheses next to the element denote the trace element isotope that was analysed. *n* = number of shards analysed. EPMA operating conditions: two sets of column conditions were utilized within the EPMA analysis. First, Na, Al, Si, K, Ca, Mg and Fe were determined using an accelerating voltage of 15 kV and a beam current of 2 nA. F, Cl, P, S, Ti and Mn were then determined using an accelerating voltage of 15 kV and a beam current of 80 nA. A 5-μm electron beam diameter was used throughout. Counting times were 20 s at the peak position and 10 s for background for all elements except F (50 and 40 s), Ti (30 and 15 s), Mn (50 and 40 s) and Fe (40 and 20 s). LA-ICP-MS operating conditions: for these analyses a laser beam diameter of 10 or 20 μm (depending on the size of shard sections) pulsed at a frequency of 5 Hz with a fluence of 10 J cm^{-2} and a flash duration of ~ 20 ns was utilized. Analyses took ~30 s and argon was used as the carrier gas. Isotopes used for analysis are given for each element. Typical instrument operating conditions are listed in Pearce *et al.* (2011).

processes (Austin *et al.*, 2004; Brendryen *et al.*, 2010; Abbott *et al.*, 2011). It is crucial, therefore, that any geochemical datasets from marine horizons that display heterogeneity are screened for 'analytical' outliers before they are interpreted for their palaeosignificance. Analytical anomalies primarily result from the influence of microphenocryst/microlite inclusions within the glass on individual analyses (Hunt and Hill, 2001). Microphenocrysts can occur within tephra shards and if wholly analysed will produce characterizations radically different from the juvenile glass of the tephra deposit and are thus readily identified during routine screening of analyses (Kuehn *et al.*, 2011). Large crystals were avoided by either observing shards under a light microscope or using back scatter electron (BSE) imagery during EPMA analysis. However, sub-surface or very small microphenocrysts may not be detected during visual or BSE inspection. Furthermore, microphenocrysts close to the analysis volume can still affect X-ray absorption and secondary fluorescence effects in EPMA (Hunt and Hill, 2001; Platz *et al.*, 2007; Kuehn *et al.*, 2011). The volume analysed during LA-ICP-MS is larger than EPMA, and thus there is an increased likelihood of microphenocryts affecting trace element characterizations of individual shards. Therefore, LA-ICP-MS data from shards outlying the main major element geochemical population at a specific depth were inspected for anomalous results (e.g. high Sr from a feldspar inclusion) to determine if the presence of a microphenocryst had contributed to the X-ray signal during the EPMA. Any 'analytical' outliers that were identified were excluded from further analysis and the reasons for exclusion are explained below and in Tables S4–S6.

Results

Tephrostratigraphy

The tephrostratigraphy for MD04-2822 between the depths of 2200 and 2700 cm is presented in Fig. 2. The two distinct peaks observed above 2380 cm are the MD04-2822 2327–2328 cm and 2359–2366 cm tephra horizons described in Abbott *et al.* (2011). Below these depths, four sections (2380–2390, 2420–2430, 2470–2500 and 2520–2530 cm) exhibited distinct peaks in colourless shards relative to background values at a 10-cm resolution and were consequentially resampled and analysed at a 1-cm resolution. Shard counts for the 80–125 μm grain-size fraction are relatively low (<30 shards) with only the 2480–2490 cm section exhibiting high concentrations (Fig. 2iv). This coincides with the highest shard concentrations (372 shards per 0.5 gdw) in the fine-grained 25–80 μm fraction and a limited number of colourless shards were identified in the >125 μm fraction. When assessed at a 1-cm resolution (Fig. 2), shard concentration peaks for the lower three horizons can be identified at 2385–2386, 2424–2425 and 2490–2491 cm, respectively, and are taken as the stratigraphic level for the isochrons. The 1-cm concentration profiles are relatively consistent between the 25–80 and 80–125 μm grain-size fractions.

For two of the sections investigated at 1 cm resolution there are apparent mismatches between the 10-cm and 1-cm counts. For 2420–2430 cm the shard counts are enhanced at the 1-cm resolution (198 shards per 0.5 gdw) compared with the 10 cm counts (54 shards per 0.5 gdw) while the section between 2480 and 2490 cm, which has a shard concentration of 372 shards per 0.5 gdw at the 10-cm resolution, shows lower counts at a 1-cm resolution, 151 shards per 0.5 gdw. This may be due to uneven distribution of tephra across the core and/or the presence of small tephra lenses. Slightly elevated shard concentrations (17 shards per 0.5 gdw) were

observed in the 10-cm sample from 2520 to 2530 cm. When investigated at a 1-cm resolution, however, only a very limited number of shards were identified in all grain size fractions. This analysis was repeated and similar concentrations were observed; therefore, no further investigation of this peak was undertaken.

Brown glass shards were present throughout the studied section, but they were present at low concentrations of less than 35 shards per 0.5 gdw (Fig. 2iv), and no distinct concentration peaks were identified. This is interpreted as representing a background of basaltic material within the marine sediments and therefore was not investigated further.

Tephra horizons and geochemical characterizations

Material was extracted for both major and trace element geochemical analysis from the three shard concentration peaks, 2385–2386, 2424–2425 and 2490–2491 cm. A distinct dominant geochemical population can be identified within all the datasets.

MD04-2822 2385–2386 cm

This tephra deposit is composed mainly of platy shards with some exhibiting a fluted morphology. Shards range in size between 40 and 225 μm with a peak in shard size around 75 μm (Fig. 3). This horizon was deposited during a warm period in MIS 5a, correlated to Greenland Interstadial (GI) 21, and based on the chronology from the core can be assigned an age of 79 600 ± 2000 a b2k. Deposition of this material did not occur with an accompanying peak in IRD flux (Fig. 2).

In total, 12 shards were analysed for their major and trace element composition and were found to have a rhyolitic composition, with 10 shards forming a distinct homogenous population (Fig. 4a). Tephra shards within the main population display SiO_2 values between ~73.5 and 74.2 wt%, FeO concentrations between 2.26 and 2.61 w%t, Na_2O concentrations of ~5 wt% and K_2O values of approximately 3.9 wt %. Comparison to proximal Icelandic material demonstrates that the main geochemical population has affinities with the transitional alkali rock suite, as the total alkali and silica values fall within the typical range for this suite and potassium enrichment values exceed 0.045 (see Lacasse and Garbe-Schönberg, 2001). These characterizations are typical of material sourced from an off-rift volcanic system (Fig. 4b; Lacasse and Garbe-Schönberg, 2001). Trace element characterizations of this main population display rare earth element (REE) profiles akin to Icelandic proximal material, with a steep gradient for the light REEs (LREE; La–Nd), a relatively flat profile for the heavy REEs (HREE; Sm–Lu) and a distinct negative Eu-anomaly (Fig. 5ai; Óskarsson *et al.*, 1982). The trace elements display reasonable homogeneity, which is more distinct for the LREEs than the heavier elements due to the better precision associated with the determination of the abundant elements (see Pearce *et al.*, 2011).

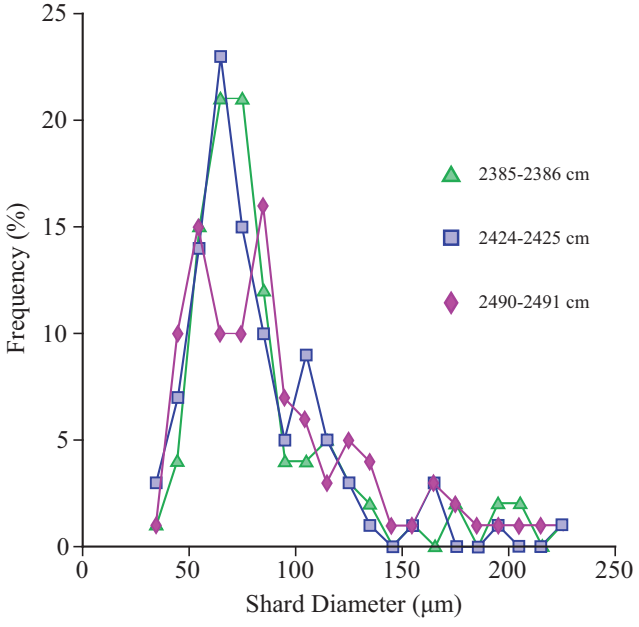

Figure 3. Frequency distribution of shard long axis diameters within the three tephra deposits. This figure is available in colour online at wileyonlinelibrary.com.

Of the outlying analyses one displays high Zr, Hf and HREE concentrations, indicating that trace element analysis of the shard included a zircon (Table S4; see Pearce *et al.*, 2002). This may have had an impact on the major element analysis and this shard is excluded. The other outlier has no characteristics associated with inclusion of mineral grains during analysis and may thus derive from either a roughly coeval eruption or, more likely, the movement of material from a past eruption by bottom currents. The dominance of the main population allows this deposit to be classified as having a homogeneous composition.

MD04-2822 2424–2425 cm

Between 2420 and 2430 cm, a relatively discrete tephra deposit with a peak in shard concentrations at 2424–2425 cm was identified. Proxy evidence from the core demonstrates that this horizon was deposited during a warm period correlated to Greenland Interstadial 22 and towards the end of the MIS 5c period. Based on this correlation, the peak in shard concentration can be assigned an age of 91 320 ± 2410 a b2k. Shard morphology in the peak sample is predominantly platy with shards ranging in size between 30 and 195 μm with a peak in shard diameters at 62.5 μm. The peak in shard concentration does not coincide with increased IRD flux (Fig. 2).

Major element analysis demonstrates that all the analysed shards are rhyolitic with one main geochemical population apparent alongside eight outlying analyses (Table S5). Shard analyses from the main population display SiO_2 concentrations between 73.2 and 74.8 wt%, Al_2O_3 concentrations of ~12.8 wt%, FeO concentrations between 2.06 and 2.89 wt%, and potassium enrichment values above 0.045. This fingerprint is characteristic of Icelandic material with a transitional alkali composition (Fig. 4bii). As with MD04-2822 2385–2386 cm, trace element characterizations of material from this main population have an REE profile similar to proximal Icelandic deposits and are relatively homogeneous (Fig. 5aii).

An assessment of the trace element composition of the outlier shards demonstrates that two may have been affected by zircon inclusions and four by plagioclase inclusions, due to high Zr and high Sr and CaO concentrations for these shards, respectively (Table S5). The remaining two outlier shards appear unaffected by analytical issues and thus may derive from similarly timed eruptions or the movement of material from past eruptions by bottom current reworking. With only two true outliers from the main population (80% of the analysed shards) the deposit can be considered to not display significant heterogeneity.

MD04-2822 2490–2491 cm

Tephra shards are dispersed over approximately 25 cm within the core, but a clear peak can be identified at 2490–2491 cm

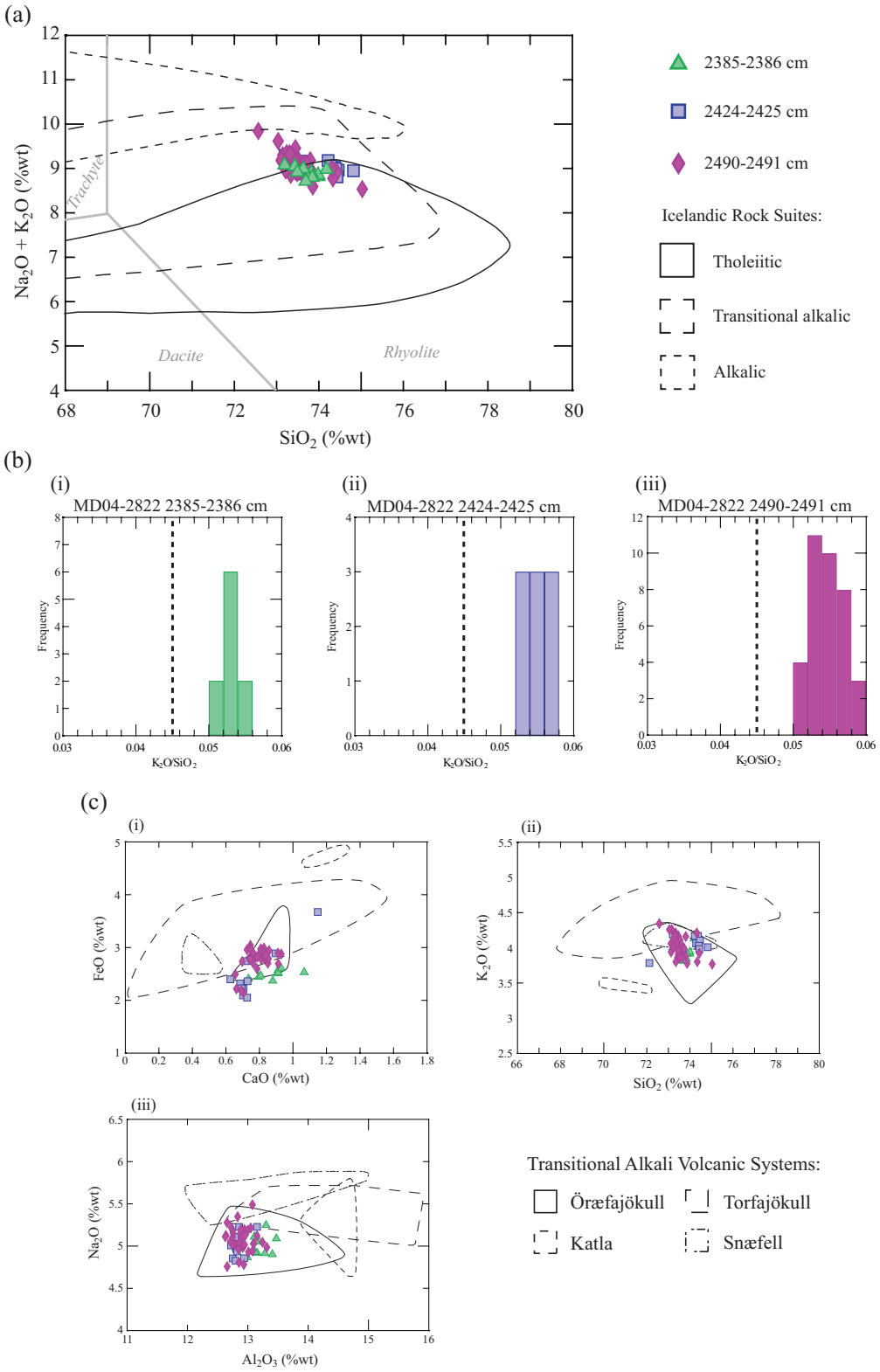

Figure 4. (a) Total alkali versus silica plot for the three tephra deposits. Geochemical fields for the Icelandic rock suites from Jakobsson *et al.* (2008). Geochemical classification and nomenclature after Le Maitre *et al.* (1989). (b) Histograms of the potassium enrichment within individual shards from the three deposits. (c) (i) CaO vs. FeO, (ii) SiO_2 vs. K_2O and (iii) Al_2O_3 vs. Na_2O major element compositional variation diagrams comparing the major element characterizations of the three main populations to geochemical fields for the silicic products of four major Icelandic transitional alkali volcanic systems. Geochemical fields defined using individual silicic rock analyses reported by Jónasson (2007). Outlying analyses have been removed from these diagrams, but are included in supporting Tables S4–S6. This figure is available in colour online at wileyonlinelibrary.com.

depth (Fig. 2). This material was deposited at the MIS 5e to 5d transition and at the end of a plateau of low *N. pachyderma* (sinistral) concentrations and a period of increased Ca concentrations related to the last interglacial period (Fig. 2i). The peak in shard deposition can be assigned an age of 116 400 ± 4000 a b2k. Material from this peak is predominately platy with some fluting and shard diameters range between 35 and 250 μm. Bimodality is observed in the shard size distribution with peaks in size frequency of 50–60 and 80–90 μm (Fig. 3). Figure 2

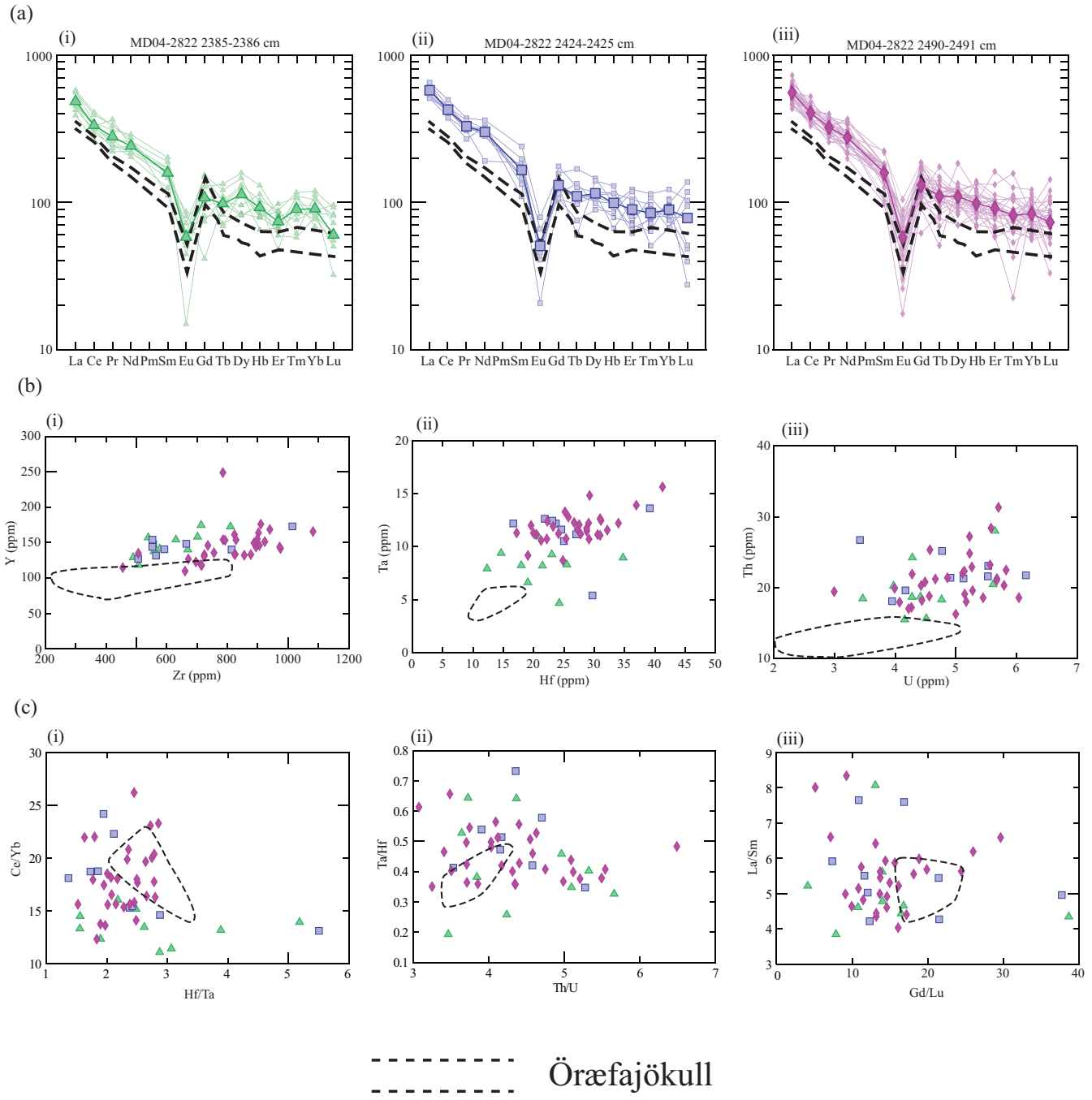

Figure 5. (a) Chondrite-normalized REE profiles for individual shard analyses and average values (bold) for the main geochemical populations of (i) MD04-2822 2385–2386 cm, (ii) MD04-2822 2424–2425 cm and (iii) MD04-2822 2490–2491 cm. Dashed line indicates the typical range of REE profiles for Öræfajökull deposits reported in Jónasson (2007). Chondrite compositions from Sun and McDonough (1989). (b) (i) Zr vs. Y, (ii) Hf vs. Ta and (iii) U vs. Th trace element compositional diagrams for the three main geochemical populations. (c) (i) Hf/Ta vs. Ce/Yb, (ii) Th/U vs. Ta/Hf and (iii) Gd/Lu vs. La/Sm trace element ratio compositional variation diagrams. Dashed line denotes the geochemical fields of trace element characterizations of proximal Öræfajökull deposits reported in Stevenson *et al.* (2006), Selbekk and Trønnes (2007) and Jónasson (2007). Outlying analyses have been removed from these diagrams, but are included in supporting Tables S4–S6. This figure is available in colour online at wileyonlinelibrary.com.

demonstrates that this horizon was deposited during a period of limited IRD flux.

The high shard concentrations within this deposit permitted the acquisition of a significant amount of geochemical data with major element analyses gained from over 40 single shards. Akin to the other deposits, all the analysed material is rhyolitic in composition with a dominant population and some outlying analyses. Three of the outliers can be excluded due to the potential influence of zircon on one analysis and plagioclase inclusions within the remaining two shards.

Overall, the deposit displays a high degree of homogeneity with 90% of the remaining analyses forming a main population. This material has SiO_2 concentrations between 73 and 75 wt%, FeO values of ~2.8 wt%, K_2O values between 3.77 and 4.35 wt% and Al_2O_3 concentrations of ~12.9 wt%. The total alkali and silica concentrations and potassium enrichment values in excess of 0.045 indicate that this material has an affinity to the Icelandic transitional alkali rock suite (Fig. 4a,b). Trace element characterizations of shards from this main population display similarities to proximal Icelandic material with similar REE profiles of a

steep gradient for the LREEs, a distinct negative Eu-anomaly and a relatively flat profile for the HREEs (Fig. 5aiii). The homogeneity displayed within the major element analyses from this population is also reflected in these trace element characterizations.

Comparison to volcanic source regions and tephra horizons in other palaeoclimatic records

Comparison of the three main geochemical populations to major element fields defined for four main Icelandic transitional alkali volcanic centres from Jónasson (2007) highlights that they all have strong affinities to the Öræfajökull system (Fig. 4c). This is also the most likely source of the tephra horizon at 2327–2328 cm depth, previously described in Abbott *et al*. (2011).

To further test this potential correlation, comparisons of the trace element characterizations of the MD04-2822 horizons to analyses of proximal material from the Öræfajökull system have been made (Fig. 5). Average REE profiles for the three main populations described here show a similar shape to proximal Öræfajökull material but the concentrations are consistently higher (Fig. 5a). This relationship is also observed on biplots of lighter and heavier elements (Fig. 5b), although similar ratio trends can be observed on these plots and overlaps on ratio/ratio biplots (Fig. 5c). The varying degree of heterogeneity observed in these datasets (Fig. 5c) may reflect the low number of characterizations used to define the Öræfajökull envelope or to the greater heterogeneity captured by single-grain LA-ICP-MS analysis as opposed to the single values provided by bulk analyses. The bulk analyses of proximal deposits presented in Stevenson *et al*. (2006), Jónasson (2007) and Selbekk and Trønnes (2007) are more likely to have incorporated material, such as feldspars, zircons and plagioclase, in addition to the juvenile glass analysed by LA-ICP-MS in this study. Bulk analyses, which will include phenocrysts and lithic phases, will have lower concentrations of incompatible elements, such as the REE and high field strength elements (HFSE), and potentially higher concentrations of compatible elements (e.g Sr) than the juvenile glass (which represents the coeval magma). Because of this behaviour, individual element concentrations vary in a predictable manner (see Pearce *et al*., 2002) but ratios of incompatible elements will be the same between bulk sample and glass shard analyses. Therefore, the similarities in REE profile shape and element ratios demonstrate that Öræfajökull cannot be ruled out as a potential source based upon the trace element data, although the trace element comparison cannot be used as supporting evidence for a correlation as a direct comparison has not been made, which would require proximal glass-phase analysis. This is required for material from various sites proximal to Icelandic volcanic systems if trace element analyses are to be consistently used to test major element-based source attributions.

An initial geochemical comparison of the MD04-2822 horizons to rhyolitic tephra deposits identified in other MIS 5 sequences rules out several potential correlatives (Fig. 6a). However, three horizons (4-DO19/RHY-I, 5d-Low/RHY-I and 5e-Top/RHY) display consistent geochemical similarities which are most apparent on the Ca vs. Fe biplot (Fig. 6b). Statistical comparisons of these different horizons were made using the statistical distance function developed by Perkins *et al*. (1995, 1998) and the similarity coefficient outlined by Borchardt *et al*. (1972) (Table 2). The characterizations of both 5d-Low/RHY-I and 5e-Top/RHY, identified in the ENAM33 core from the Faroe Island region by Wastegård and Rasmussen (2001), are shown to be statistically different from the three MD04-2822 horizons. This observation is also supported by low similarity coefficient values for comparisons between these horizons (Table 2ii). Thus, despite these two horizons having stratigraphic similarities to the MD04-2822 2490–2491 cm horizon, which also falls around the MIS 5e/5d transition, a secure correlation between the sequences cannot be defined.

The 4-DO19/RHY-I horizon identified in the MD99-2289 core from the Norwegian Sea and reported by Brendryen *et al*. (2010) shows geochemical similarities to all the MD04-2822 horizons with the D^2 values falling below the critical value and all the similarity coefficients exceeding 0.95. However, according to the stratigraphic and chronological framework of Brendryen *et al*. (2010) the 4-DO19/RHY-I horizon was deposited during MIS 4 after GI-19 and has been assigned an age of 70.1 ka. This is significantly younger than and stratigraphically distinct from all the MIS 5 MD04-2822 horizons. The strong geochemical affinities may instead reflect the horizons having a common source (i.e. Öræfajökull) rather than originating from a common volcanic event. This would contradict the attribution of 4-DO19/RHY-I to a Torfajökull source by Brendryen *et al*. (2010), but these systems do have overlapping geochemical envelopes (Fig. 4), which could also account for high similarity coefficient values.

Comparison to Icelandic terrestrial deposits

Despite the inconclusive correlations to previously published tephra horizons, a correlation to deposits in Iceland may well be possible. Five terrestrial deposits from the Western Rift Zone, Kerlingarfjöll and Torfajökull with Ar–Ar ages that fall within the MIS 4–6 interval have been identified and described by McGarvie *et al*. (2006, 2007) and Flude *et al*. (2010). The large errors associated with these ages mean that many overlap with the ages assigned to one or more of the five tephra horizons identified in MD04-2822 in this study and Abbott *et al*. (2011) (Fig. 7). Whole rocks from these proximal deposits have been analysed using XRF to characterize their major and trace element geochemistry and are compared with geochemical envelopes for the MD04-2822 horizons gained from single shard analyses (Fig. 8). For the major element comparisons (Fig. 8a), consistent affinities are seen between two terrestrial deposits and two MD04-2822 horizons. The tholeiitic 2359–2366 cm horizon (Abbott *et al*., 2011) and the Prestahnúkur deposit in Iceland's Western Rift Zone described by McGarvie *et al*. (2007) and the transitional alkali 2385–2386 cm horizon and the Hverahnukur deposit identified in the Kerlingarfjöll volcanic zone by Flude *et al*. (2010) show overlapping major element compositions. Geochemical similarities between these pairs are also observed in the trace element characterizations (Fig. 8b), notably in ratio trends (Fig. 8b, i) and for the Rb/Sr and Y/Zr element ratios (Fig. 8b, ii). As with the trace element comparison to proximal Öræfajökull deposits one would expect concentration differences with analyses of proximal (bulk) deposits exceeding analyses of distal (single glass shards) material, but a consistency in trace element ratios should exist within rhyolitic magmas. The ages assigned to these pairs of horizons overlap (Prestahnúkur deposit: 89 ± 24 ka vs. MD04-2822 2359–2366 cm: 73 420 $\pm$ 1770 a b2k and Hverahnukur deposit: 68 ± 21 ka vs. MD04-2822 2385–2386 cm horizon: 79 600 $\pm$ 2000 a b2k; Fig. 7). We are fully aware, however, that the large uncertainties on these Ar–Ar ages provide only weak support for these correlations. In addition, it is questionable whether the eruptions that produced the proximal deposits became subaerial and

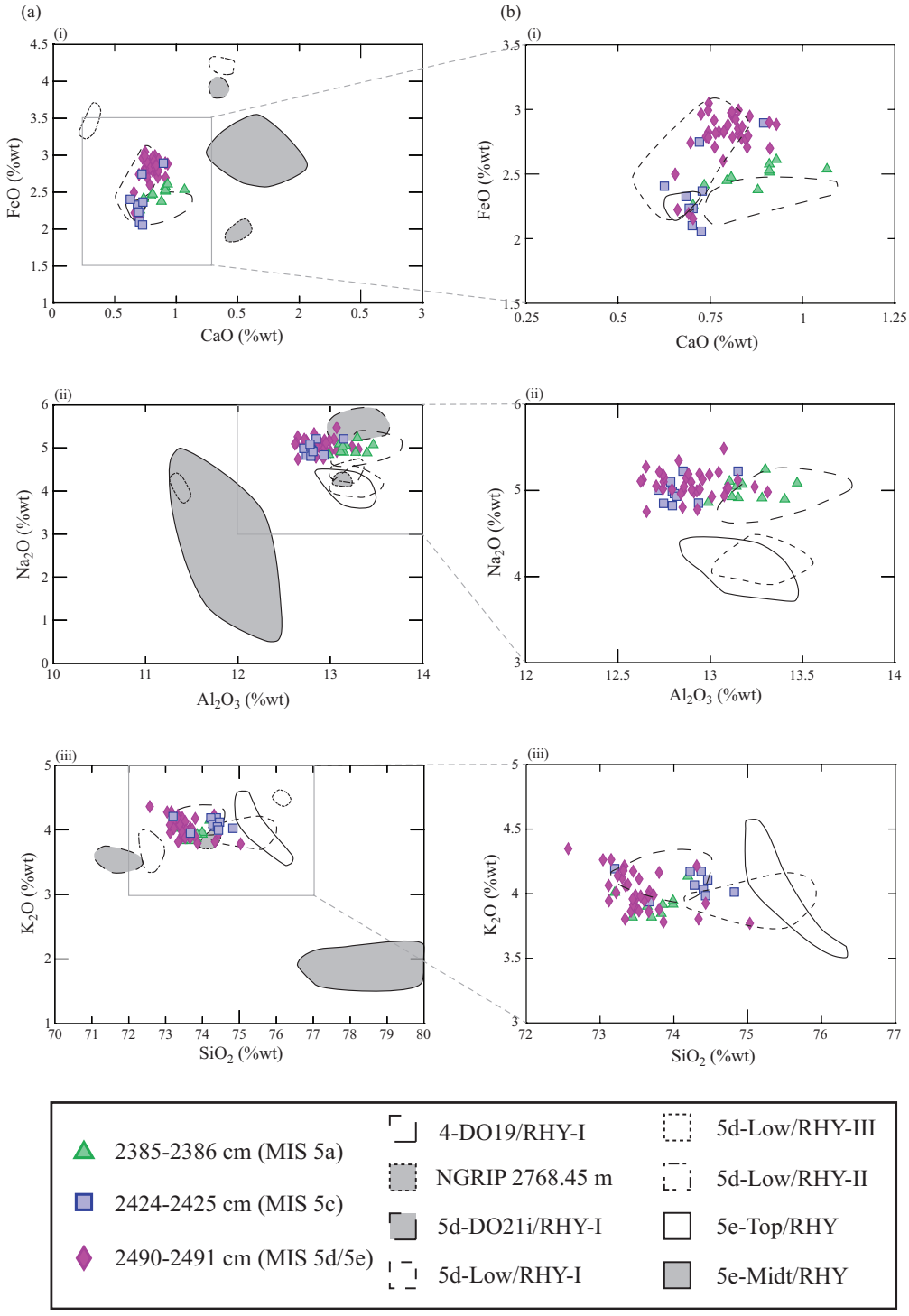

Figure 6. Geochemical comparison of individual shard analyses from the main populations of the three MD04-2822 tephra deposits to geochemical fields for eight MIS 4–6 rhyolitic horizons identified in other palaeoclimatic sequences from the North Atlantic region. NGRIP 2768.45 m reported in Abbott *et al.* (2012), 4-DO19/RHY-I, 5d-DO21i/RHY-I, 5d-Low/RHY-I, -II, -III described in Brendryen *et al.* (2010) and 5e-Top/RHY described in Wastegård and Rasmussen (2001). Geochemical field for 5e-Midt/RHY utilized data from Fronval *et al.* (1998), Brendryen *et al.* (2010) and Wastegård and Rasmussen (2001). This figure is available in colour online at wileyonlinelibrary.com.

dispersed ash into the atmosphere and, furthermore, there are numerous proximal deposits that are yet to be Ar–Ar dated (McGarvie, 2009), including ones associated with the Öræfajökull volcanic system (Walker *et al.*, 2010). The latter issue may explain why these correlations would contradict the attribution of the eruptions to the Öræfajökull volcanic system. Overall, the correlations proposed here should be classed as highly tentative, although there is clearly considerable potential for establishing Icelandic terrestrial to North Atlantic marine correlations during this period.

Discussion

Geochemical characteristics of tephra horizons

A striking feature of the three MIS 5 horizons is their close geochemical similarity (Fig. 4), and the strong affinity to an Öræfajökull source suggests that this volcanic system was highly active during this period. Tracing these horizons into other palaeoclimatic sequences will rely heavily on geochemical correlation and using characterizations to discriminate between the different Öræfajökull eruptions. While there are

Table 2. Statistical distance and similarity coefficient comparisons.

	4-DO19/RHY-I	5d-Low/RHY-I	5e-Top/RHY
(i) Statistical distance comparisons			
2385–2386 cm	8.653*	27.702	28.973
2424–2425 cm	16.186*	30.180	19.148
2490–2491 cm	12.880*	31.336	33.845
(ii) Similarity coefficient comparisons			
2385–2386 cm	0.961*	0.932	0.908
2424–2425 cm	0.963*	0.947	0.942
2490–2491 cm	0.951*	0.926	0.901

(i) Statistical distance comparisons between the average geochemical composition of three MD04-2822 tephra horizons and three MIS 4–6 horizons identified in other North Atlantic marine sequences. Asterisk (*) denotes values that do not exceed the critical value of 18.48 and thus cannot be regarded as being statistically different. (ii) Similarity coefficient comparisons between the average geochemical composition of three MD04-2822 tephra horizons and three MIS 4–6 horizons identified in other North Atlantic marine sequences. Asterisk (*) denotes value that fall above the threshold of 0.95 which if exceeded indicates that the horizons could have an identical composition (see Begét *et al.*, 1992).

broad similarities between the three MIS 5 horizons, some key discriminatory features are evident. For example, MD04-2822 2490–2491 cm can be distinguished from the other two horizons based on higher FeO (Fig. 6bi) and TiO_2 values in addition to a different trend in Y/Zr ratios (Fig. 5bi). In addition, higher Al_2O_3 values for the MD04-2822 2385–2386 cm shards permits their differentiation from MD04-2822 2424–2425 cm (Fig. 6bii). These subtleties will be key if the potential arises to trace these horizons into other sequences.

The use of trace element characterizations within distal tephrochronological studies is limited at present but is increasing (e.g. Abbott *et al.*, 2012; Davies *et al.*, 2012; Lane *et al.*, 2012; Albert *et al.*, 2012). Trace element analyses have the potential to provide a secondary check of proximal–distal and distal–distal correlations and aid in the discrimination of horizons with similar major element compositions. The reporting of the characterizations of the MD04-2822 horizons here adds to the present framework and will be valuable if future studies incorporate trace element analysis. As shown earlier, the use of these data within the determination of the volcanic source of eruptions is complex and may require the development of comprehensive LA-ICP-MS trace element datasets of proximal glass material so that direct comparisons can be performed.

Transportation and reworking of tephra horizons

Determining the processes responsible for the transport and deposition of tephra within marine sequences is crucial to assess their potential value as isochronous markers for correlation and synchronization purposes. Three potential mechanisms were in operation within the glacial North Atlantic: iceberg rafting, sea-ice rafting and primary airfall. Geochemical data, shard-size data and IRD flux are used to assess the dominant processes at the time the MD04-2822 horizons were deposited. Figure 2 demonstrates that none of the horizons was deposited during periods of increased IRD flux, providing strong evidence that the tephra shards were not deposited at a time of intense iceberg rafting. The relative geochemical homogeneity (Figs. 4 and 5) and well-sorted shard-size distributions (Fig. 3) also point towards transport via primary airfall and, potentially, sea-ice rafting processes. Both mechanisms are thought to transport and deposit material within very short time-intervals, with sea-ice rafted material thought to be deposited within months to a few years, and hence are insignificant on geological time frames (Brendryen *et al.*, 2010).

Sea-ice rafting has the potential to transport material larger than expected to distal sites. For example, shards 200 μm in diameter and related to North Atlantic Ash Zone II are thought to have been transported to the MD95-2006 site only 83 km away from the MD04-2822 core location (Austin *et al.*, 2004). The peak in shard size for each of the MIS 5 horizons in MD04-2822 was around 70 μm with few shards >150 μm identified. The size distribution of these three horizons is consistent with material deposited in terrestrial sequences, such as Scottish lake sequences, which could suggest the material was transported to the MD04-2822 site via primary airfall. This size distribution could also arise through sea-ice rafting, with smaller material deposited on sea-ice in locations downwind from the volcanic source before rafting. Thus, overall the characteristics of the MIS 5 tephra deposits and associated proxy evidence demonstrate that the material was most likely transported via primary airfall, akin to the two previously identified MIS 4 horizons, although sea-ice rafting cannot be wholly ruled out (Abbott *et al.*, 2011).

Reworking due to bioturbation, bottom currents and gravity-driven sediment flows can also affect the stratigraphic integrity of a tephra horizon and the 'true' position of an isochron. In this study the position of the isochron has been defined as the peak in shard concentration as this is commonly interpreted to represent the 'exact' timing of the eruption (Davies *et al.*, 2012). Of the three MIS 5 horizons, both MD04-2822 2385–2386 cm and MD04-2822 2424–2425 cm do not display single large peaks at a 1-cm resolution; both, however, are well constrained with distinct shard concentration increases spanning <10 cm depth. This suggests some reworking has occurred, with some upward migration of shards due to bioturbation and downward migration due to bioturbation and/or the settling of particles through soft-sediment (Enache and Cumming, 2006; Payne and Gehrels, 2010). However, these processes are considered to have had a limited impact on the depth and value of the isochron. MD04-2822 2490–2491 cm is relatively dispersed within the sequence with a complex shard concentration profile stretching over 25 cm with a distinct upward tail (Fig. 2). The greater dispersal and tail may be due to increased bioturbation resulting from increased productivity (e.g. Jumars and Wheatcroft, 1989) during this period or potentially resulted from a series of closely timed eruptions. Despite this observation, the peak at 2490–2491 cm depth is more distinct than the other horizons and can be reliably used as the isochron position. The presence of shards outlying the main geochemical populations of all three horizons may indicate material from past eruptions being reworked by bottom currents, although their low number suggests that this process had a limited impact. The occurrence of a series of horizons with similar geochemistry could imply that material from one eruption has been repeatedly overlain at the site, but this seems unlikely given the slight differences in geochemistry that can be observed between the horizons and the integrity of the climate record.

Having considered the evidence, it seems unlikely that there was a significant temporal delay between the eruption that produced the tephra horizons and their deposition at the MD04-2822 core site. Thus, we conclude that these can be utilized as isochronous horizons for the linking of palaeoclimatic sequences. Although this has not been achieved in

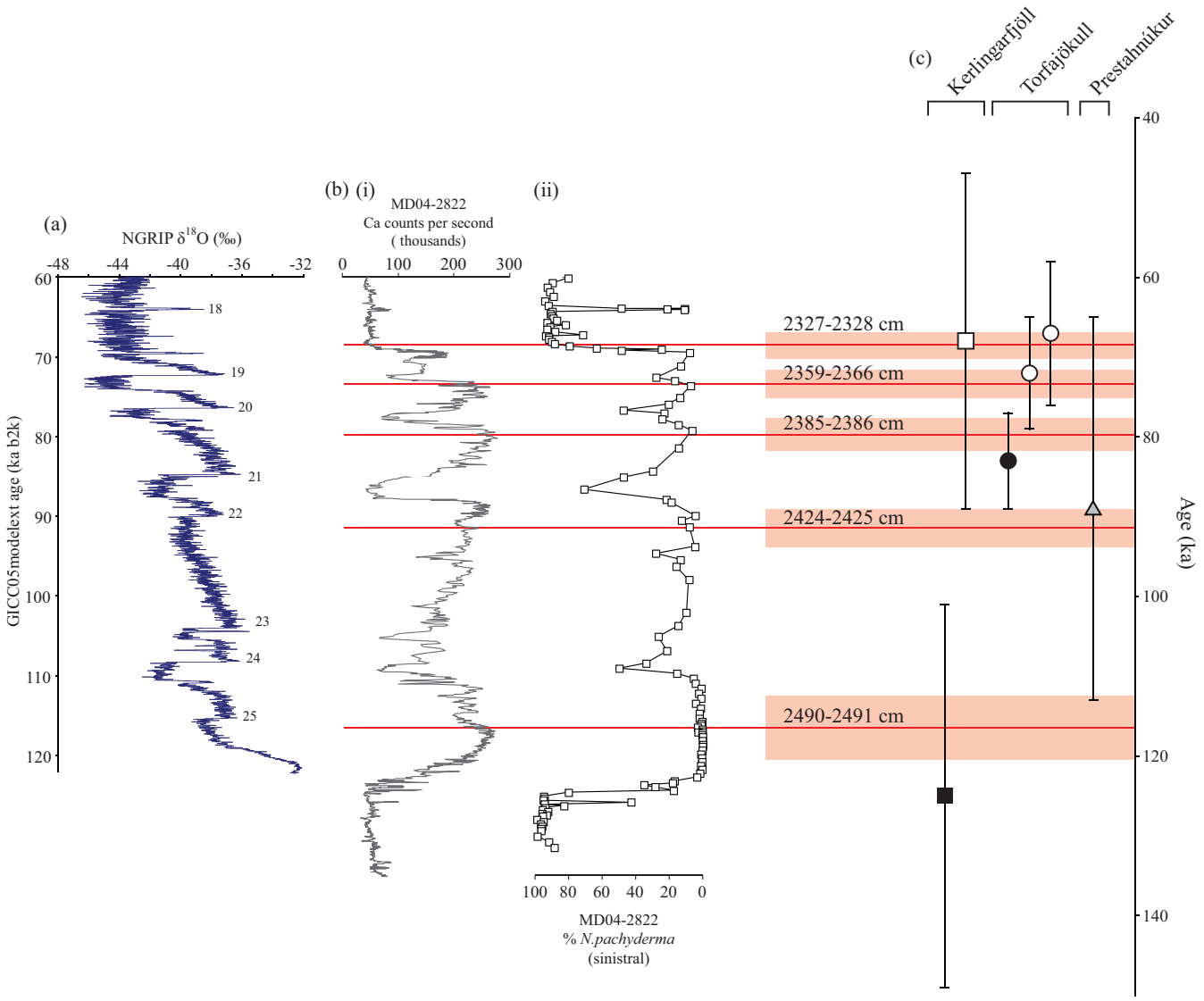

Figure 7. Comparison of age estimates for all MD04-2822 MIS 4–6 horizons and proximal Icelandic deposits. (a) Oxygen isotope ratio variations from the NGRIP ice-core (North Greenland Ice Core Project Members, 2004; Svensson *et al.*, 2008; Wolff *et al.*, 2010). (b) (i) XRF (ITRAX core scanning) Ca count rates and (ii) high-resolution percentage abundance of *N. pachyderma* (sinistral) plotted on the revised chronology for MD04-2822. (c) Ar–Ar ages for Icelandic terrestrial deposits from the Kerlingarfjöll (Flude *et al.*, 2010), Torfajökull (McGarvie *et al.*, 2006) and Prestahnúkur (McGarvie *et al.*, 2007) volcanic systems. Symbols are consistent with those used on Fig. 8. Red lines denote the stratigraphic position of the MD04-2822 tephra horizons and red shaded areas denote the uncertainties on the age estimates. This figure is available in colour online at wileyonlinelibrary.com.

this study, their recognition within the high-resolution stratigraphy of MD04-2822 could aid their identification in other palaeoclimatic sequences through targeting of specific coeval intervals. The linking of sequences using common tephra horizons could be crucial to understanding the phasing of past climatic change and these horizons all fall during a period characterized by rapid shifts in climate (Fig. 2). The MD04-2822 2385–2386 cm horizon could be a useful tie-line, as it is relatively well constrained within the sequence, falling just before a cooling transition recorded in the *N. pachyderma* records that has been correlated to the transition between GI-21 and GS-21 as recorded in the NGRIP ice-core (Fig. 7).

MIS 5 North Atlantic tephrostratigraphy

None of the MIS 5 tephra horizons identified within MD04-2822 can be correlated to previously published horizons and thus are all new additions to the North Atlantic framework of volcanic events during this period. Most striking is that although the 5e-Midt/RHY forms a key marker horizon for the Eemian period, having been previously isolated within cores from north of Iceland (Sejrup *et al.*, 1989; Sjøholm *et al.*, 1991; Fronval *et al.*, 1998), the MD95-2009 Faroe Islands region core (Rasmussen *et al.*, 1999; Wastegård and Rasmussen, 2001), the Norwegian Sea (Brendryen *et al.*, 2010) and a terrestrial sequence on the Faroe Islands (Wastegård *et al.*, 2005), this horizon was not isolated in the MD04-2822 core. A small shard concentration peak was identified in MIS 5e, between 2520 and 2530 cm depth, but no significant tephra concentrations were observed in repeated inspection of 1-cm samples. These previous studies have not interpreted 5e-Midt/RHY as an ice-rafted deposit but as airfall transported. It is possible that its non-identification in MD04-2822 implies that the plume from this eruption transported material north and west of Iceland, but not as far south as the MD04-2822 depositional site. This may also explain why it was identified in the MD95-2009 core by Wastegård and Rasmussen (2001) and not the more southerly ENAM33 (Fig. 1).

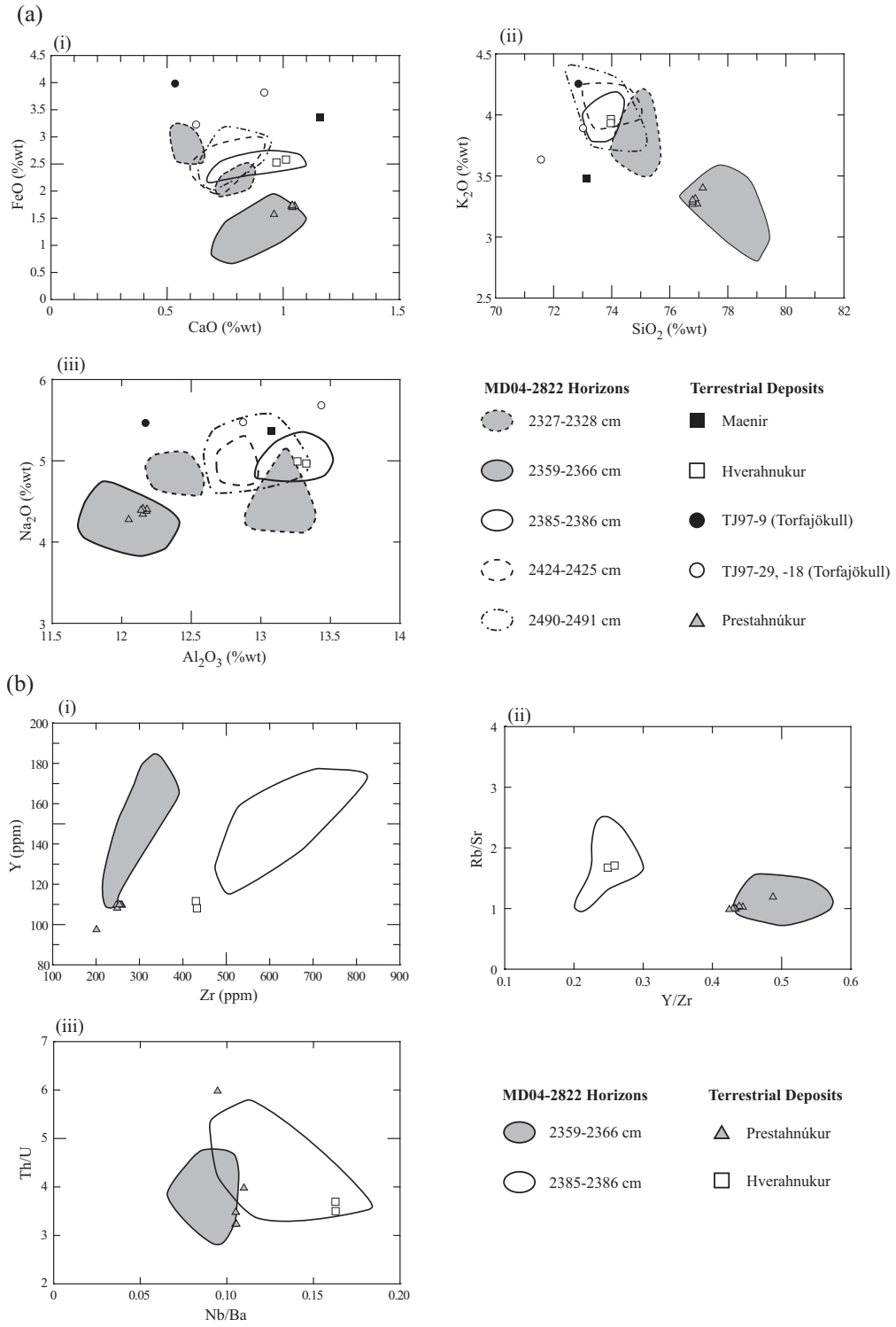

Figure 8. Comparisons of geochemical envelopes for the five MD04-2822 horizons to geochemical characterizations of Ar–Ar-dated Icelandic terrestrial deposits with ages that fall within the range of MIS 4–6. (a) (i) CaO vs. FeO, (ii) SiO_2 vs. K_2O and (iii) Al_2O_3 vs. Na_2O major element compositional variation diagrams. (b) (i) Zr vs. Y, (ii) Y/Zr vs. Rb/Sr and (iii) Nb/Ba vs. Th/U trace element compositional variation diagrams. Geochemical data for MD04-2822 horizons from this work and Abbott *et al.* (2011). Geochemical data for terrestrial deposits from McGarvie *et al.* (2006) (TJ97-9, TJ97-29, TJ97-18), McGarvie *et al.* (2007) (Prestahnúkur) and Flude *et al.* (2010) (Maenir and Hverahnukur).

Conclusions

The three identified tephra horizons represent new 'events' within the North Atlantic tephrochronological framework and the event stratigraphy for the MIS 5e-4 period. These have the potential to aid the stratigraphic correlation and age control of records covering this period (Austin and Hibbert, 2012). Age estimates for these horizons are already linked to the NGRIP GICC05 ice-core chronology based on the synchronization of MD04-2822 to the ice-core record. Should these horizons be identified in the ice-core records then this opens new possibilities for testing both the validity of the correlation based on the GI events and the assumption of synchronicity between the records. More conclusive correlation of these marine horizons to specific terrestrial deposits would also offer a means to ascribe independent Ar/Ar ages to these events, thereby providing age-control points for the marine cores that are wholly independent of the ice-core records. Although these current published ages have large uncertainties (Fig. 7), there is considerable potential to reduce these

errors with new mass spectrometry techniques (e.g. Mark *et al.*, 2009).

Supporting information

Additional supporting information may be found in the online version of this article at the publisher's web-site.

Table S1. Secondary standard analyses of the Lipari standard made throughout the analytical period of the MD04-2822 material.

Table S2. Secondary standard analyses of the BHVO-2g standard made throughout the analytical period of the MD04-2822 material.

Table S3. Trace element analytical data from USGS Glass reference materials BHVO-2G and BCR-2G.

Table S4. Major oxide and trace element concentrations of shards from the MD04-2822 2385–2386 cm sample.

Table S5. Major oxide and trace element concentrations of shards from the MD04-2822 2424–2425 cm sample.

Table S6. Major oxide and trace element concentrations of shards from the MD04-2822 2490–2491 cm sample.

Please note: This supporting information is supplied by the authors, and may be re-organized for online delivery, but is not copy-edited or typeset by Wiley-Blackwell. Technical support issues arising from supporting information (other than missing files) should be addressed to the authors.

Acknowledgements. P.M.A., S.M.D., W.E.N.A. and N.J.G.P. are supported by NERC through the SMART project (NE/F020600/1, NE/F02116X/1, NE/F021445/1). W.E.N.A. and F.D.H. acknowledge the support of NERC through British Geological Survey support and facility support via NIGL (IP898/0506). P.M.A. and S.M.D. acknowledge the support of the Climate Change Consortium of Wales (C3W). Thanks to Gareth James (Swansea University) for laboratory assistance. We thank the captain and crew of the RV *Marion Dufresne* for their assistance in recovering core MD04-2822. We are grateful for the assistance of Dr Chris Hayward using the electron microprobe at the Tephrochronology Analytical Unit, University of Edinburgh. Thanks to Sean Pyne-O'Donnell and an anonymous reviewer for their comments on the manuscript. This paper contributes to the INTREPID project 'Enhancing tephrochronology as a global research tool through improved fingerprinting and correlation techniques and uncertainty modelling' – an INQUA INTAV-led project (International Focus Group on Tephrochronology and Volcanism, project No. 0907).

Abbreviations. BIIS, British and Irish Ice Sheet; BSE, back scatter electron; gdw, g dry weight; GI, Greenland Interstadial; HFSE, high field strength elements; HREE, heavy rare earth elements; IRD, ice-rafted debris; LA-ICP-MS, laser ablation inductively coupled plasma mass spectrometry; LIG, last interglacial; LREE, light rare earth elements; MIS, Marine Isotope Stage; REE, rare earth elements; WDS EPMA, wavelength-dispersive electron-probe micro-analysis.

References

Abbott PM, Davies SM, Austin WEN, Pearce NJG, Hibbert FD. 2011. Identification of cryptotephra horizons in a North East Atlantic marine record spanning marine isotope stages 4 and 5a (~60,000–82,000 a b2k). *Quaternary International* **246**: 177–189.

Abbott PM, Davies SM, Steffensen JP, Pearce NJG, Bigler M, Johnsen SJ, Seierstad IK, Svensson A, Wastegård SS. 2012. A detailed framework of marine isotope stage 4 and 5 volcanic events recorded in two Greenland ice-cores. *Quaternary Science Reviews* **36**: 59–77.

Albert PG, Tomlinson EL, Smith VC, Di Roberto A, Todman A, Rosi M, Marani M, Muller W, Menzies MM. 2012. Marine-continental tephra correlations: volcanic glass geochemistry from the Marsili Basin and the Aeolian Islands, southern Tyrrhenian Basin Sea, Italy. *Journal of Volcanology and Geothermal Research* **229–230**: 74–94.

Austin WEN, Hibbert FD. 2012. Tracing time in the ocean: a brief review of chronological constraints (60-8 kyr) on North Atlantic marine event-based stratigraphies. *Quaternary Science Reviews* **36**: 28–37.

Austin WEN, Hibbert FD, Rasmussen SO, Peters C, Abbott PM, Bryant CL. 2012. The synchronization of palaeoclimate events in the North Atlantic region during Greenland Stadial 3 (ca 27.5 to 23.3 kyr b2k). *Quaternary Science Reviews* **36**: 154–163.

Austin WEN, Wilson LJ, Hunt JB. 2004. The age and chronostratigraphical significance of North Atlantic Ash Zone II. *Journal of Quaternary Science* **19**: 137–146.

Begét J, Mason O, Anderson PP. 1992. Age, extent and climatic significance of the c. 3400 BP Aniakchak tephra, western Alaska, USA. *The Holocene* **2**: 51–56.

Blockley SPE, Pyne-O'Donnell SDF, Lowe JJ, Matthews IP, Stone A, Pollard AM, Turney CSM, Molyneux EG. 2005. A new and less destructive laboratory procedure for the physical separation of distal glass tephra shards from sediments. *Quaternary Science Reviews* **16–17**: 1952–1960.

Borchardt GA, Aruscavage PJ, Millard H Jr. 1972. Correlation of the Bishop ash, a Pleistocene marker bed, using instrumental neutron activation analysis. *Journal of Sedimentary Petrology* **42**: 201–206.

Brendryen J, Haflidason H, Sejrup HP. 2010. Norwegian Sea tephrostratigraphy of marine isotope stages 4 and 5: prospects and problems for tephrochronology in the North Atlantic region. *Quaternary Science Reviews* **29**: 847–864.

Capron E, Landais A, Chappellaz J, Schilt A, Buiron D, Dahl-Jensen D, Johnsen SJ, Jouzel J, Lemieux-Dudon B, Loulergue L, Leuenberger M, Masson-Delmotte V, Meyer H, Oerter H, Stenni B. 2010. Millennial and sub-millenial scale climate variations recorded in polar ice cores over the last glacial period. *Climate of the Past* **6**: 345–365.

Chapman MR, Shackleton NJ. 1999. Global ice-volume fluctuations, North Atlantic ice-rafting events, and deep-ocean circulation changes between 130 and 70 ka. *Geology* **27**: 795–798.

Davies SM, Abbott PM, Pearce NJG, Wastegård S, Blockley SPE. 2012. Integrating the INTIMATE records using tephrochronology: rising to the challenge. *Quaternary Science Reviews* **36**: 11–27.

Davies SM, Hoek WZ, Bohncke JP, Lowe JJ, Pyne-O'Donnell S, Turney CSM. 2005. Detection of Lateglacial distal tephra layers in the Netherlands. *Boreas* **34**: 123–135.

Enache MD, Cumming BF. 2006. The morphological and optical properties of volcanic glass: a tool to assess density-induced vertical migration of tephra in sediment cores. *Journal of Paleolimnology* **35**: 661–667.

Flude S, McGarvie DW, Burgess R, Tindle AG. 2010. Rhyolites at Kerlingarfjöll, Iceland: the evolution and lifespan of silicic central volcanoes. *Bulletin of Volcanology* **72**: 523–538.

Fronval T, Jansen E, Haflidason H, Sejrup HP. 1998. Variability in surface and deep water conditions in the Nordic Seas during the Last Interglacial Period. *Quaternary Science Reviews* **17**: 963–985.

Grönvold K, Óskarsson N, Johnsen SJ, Clausen HB, Hammer CU, Bond G, Bard E. 1995. Ash layers from Iceland in the Greenland GRIP ice core correlated with oceanic and land sediments. *Earth and Planetary Science Letters* **135**: 149–155.

Hayward C. 2012. High spatial resolution electron probe microanalysis of tephras and melt inclusions without beam-induced chemical modification. *The Holocene* **22**: 119–125.

Hibbert FD, Austin WEN, Leng MJ, Gatliff RW. 2010. British Ice Sheet dynamics inferred from North Atlantic ice-rafted debris records spanning the last 175,000 years. *Journal of Quaternary Science* **25**: 461–482.

Hunt JB, Hill PG. 2001. Tephrological implications of beam size-sample-size effects in electron microprobe analysis of glass shards. *Journal of Quaternary Science* **16**: 105–117.

Jakobsson SP, Jónasson K, Sigurdsson IA. 2008. The three igneous rock suites of Iceland. *Jökull* **58**: 117–138.

Jónasson KK. 2007. Silicic volcanism in Iceland: composition and distribution within the active volcanic zones. *Journal of Geodynamics* **43**: 101–117.

Jumars PA, Wheatcroft RA. 1989. Responses of benthos to changing food quality and quantity, with a focus on deposit feeding and bioturbation. In *Productivity of the Ocean: Present and Past*, Berger WH, Smetacek VS, Wefer G (eds). Wiley: New York; 235–253.

Knudsen K-L, Seidenkrantz M-S, Kristensen P. 2002. Last Interglacial and Early Glacial circulation in the northern North Atlantic Ocean. *Quaternary Research* **58**: 22–26.

Kuehn SC, Froese DG, Shane PAR. INTAV Intercomparison Participants. 2011. The INTAV intercomparison of electron-beam microanalysis of glass by tephrochronology laboratories: results and recommendations. *Quaternary International* **246**: 19–47.

Lacasse C, Carey S, Sigurdsson H. 1998. Volcanogenic sedimentation in the Iceland Basin: influence of subaerial and subglacial eruptions. *Journal of Volcanology and Geothermal Research* **83**: 47–73.

Lacasse C, Garbe-Schönberg C-D. 2001. Explosive volcanism on Iceland and the Jan Mayen area during the last 6Ma: sources and timing of major eruptions. *Journal of Volcanology and Geothermal Research* **107**: 113–147.

Lane CS, Blockley SPE, Mangerud J, Smith VC, Lohne ØS, Tomlinson EL, Matthews IP, Lotter AF. 2012. Was the 12.1 ka Icelandic Vedde Ash one of a kind? *Quaternary Science Reviews* **33**: 87–99.

Le Maitre RW, Bateman P, Dudek A, Keller J, Lameyre PA, Le Bas MJ, Sabine PA, Schmid R, Sorensen H, Streckeisen A, Woolley AR, Zanettin B. 1989. *A Classification of Igneous Rocks and Glossary of Terms*. Blackwell Publishing: Oxford.

Lisiecki LE, Raymo ME. 2005. A Pliocene–Pleistocene stack of 57 globally distributed benthic $\delta^{18}O$ records. *Paleoceanography* **20**: PA1003.

Lototskaya A, Ganssen GM. 1999. The structure of Termination II (penultimate deglaciation and Eemian) in the North Atlantic. *Quaternary Science Reviews* **18**: 1641–1654.

Mark D, Barfod D, Stuart FM, Imlach J. 2009. The Argus multi-collector noble gas mass spectrometer: performance for $^{40}Ar/^{39}Ar$ geochronology. *Geochemistry, Geophysics, Geosystems* **10**: Q0A–A02.

McGarvie DW. 2009. Rhyolitic volcano-ice interactions in Iceland. *Journal of Volcanology and Geothermal Research* **185**: 367–389.

McGarvie DW, Burgess R, Tindle AG, Tuffen H, Stevenson JA. 2006. Pleistocene rhyolitic volcanism at Torfajökull, Iceland: eruption ages, glaciovolcanism, and geochemical evolution. *Jökull* **56**: 57–75.

McGarvie DW, Stevenson JA, Burgess R, Tuffen H, Tindle AG. 2007. Volcano-ice interactions at Prestahnúkur, Iceland: rhyolite eruption during the last interglacial–glacial transition. *Annals of Glaciology* **45**: 38–47.

McManus JF, Bond GC, Broecker WS, Johnsen SJ, Labeyrie L, Higgins S. 1994. High-resolution climate records from the North Atlantic during the last interglacial. *Nature* **371**: 326–329.

McManus JF, Oppo DW, Cullen JL. 1999. A 0.5-million-year record of millennial-scale climate variability in the North Atlantic. *Science* **283**: 971–975.

McManus JF, Oppo DW, Keigwin LD, Cullen JL, Bond GC. 2002. Thermohaline circulation and prolonged interglacial warmth in the North Atlantic. *Quaternary Research* **58**: 17–21.

North Greenland Ice Core Project Members. 2004. High-resolution record of Northern Hemisphere climate extending into the last interglacial period. *Nature* **431**: 147–151.

Oppo DW, Keigwin LD, McManus JF, Cullen JL. 2001. Persistent suborbital climate variability in marine isotope stage 5 and Termination II. *Paleoceanography* **16**: 280–292.

Óskarsson N, Sigvaldason GE, Steinthórsson SS. 1982. A Dynamic model of Rift Zone petrogenesis and the regional petrology of Iceland. *Journal of Petrology* **23**: 28–74.

Payne R, Gehrels M. 2010. The formation of tephra layers in peatlands: an experimental approach. *Catena* **81**: 12–23.

Pearce NJG, Denton JS, Perkins WT, Westgate JA, Alloway BV. 2007. Correlation and characterisation of individual glass shards from tephra deposits using trace element laser ablation ICP-MS analyses: current status and future potential. *Journal of Quaternary Science* **22**: 721–736.

Pearce NJG, Eastwood WJ, Westgate JA, Perkins WT. 2002. Trace-element composition of single glass shards in distal Minoan tephra from SW Turkey. *Journal of the Geological Society* **159**: 545–556.

Pearce NJG, Perkins WT, Westgate JA, Gorton MP, Jackson SE, Neal CR, Chenery SP. 1997. A compilation of new and published major and trace element data for NIST SRM 610 and NIST SRM 612 glass reference materials. *Geostandards Newsletter* **21**: 115–144.

Pearce NJG, Perkins WT, Westgate JA, Wade SC. 2011. Trace-element microanalysis by LA-ICP-MS: the quest for comprehensive chemical characterisation of single, sub-10 μm volcanic glass shards. *Quaternary International* **246**: 57–81.

Perkins ME, Brown FH, Nash WP, McIntosh W, Williams SK. 1998. Sequence, age, and source of silicic fallout tuffs in middle to late Miocene basins of the northern Basin and Range province. *Bulletin of the Geological Society of America* **110**: 344–360.

Perkins ME, Nash WP, Brown FH, Fleck RJ. 1995. Fallout tuffs of Trapper Creek, Idaho – a record of Miocene explosive volcanism in the Snake River Plain volcanic province. *Bulletin of the Geological Society of America* **107**: 1484–1506.

Perkins WT, Pearce NJG. 1995. Mineral microanalysis by laserprobe inductively coupled plasma mass spectrometry. In *Microprobe Techniques in the Earth Sciences*, Potts PJ, Bowles JFW, Reed SJB, Cave MR (eds). The Mineralogical Society: London; 291–325.

Platz T, Cronin SJ, Smith IEM, Turner MB, Stewart RB. 2007. Improving the reliability of microprobe-based analyses of andesitic glasses for tephra correlation. *The Holocene* **17**: 573–583.

Rasmussen TL, Balbon E, Thomsen E, Labeyrie L, van Weering TCE. 1999. Climate records and changes in deep outflow from the Norwegian Sea ~150-55 ka. *Terra Nova* **11**: 61–66.

Rousseau D-D, Kukla G, McManus J. 2006. What is what in the ice and the ocean? *Quaternary Science Reviews* **25**: 2025–2030.

Sejrup HP, Sjøholm J, Furnes H, Beyer I, Eide L, Jansen E, Mangerud J. 1989. Quaternary tephrochronology on the Iceland Pleateau, north of Iceland. *Journal of Quaternary Science* **4**: 109–114.

Selbekk RS, Trønnes RG. 2007. The 1362 AD Öræfajökull eruption, Iceland: petrology and geochemistry of large-volume homogenous rhyolite. *Journal of Volcanology and Geothermal Research* **160**: 42–58.

Sjøholm J, Sejrup HP, Furnes H. 1991. Quaternary volcanic ash zones on the Iceland Plateau, southern Norwegian Sea. *Journal of Quaternary Science* **6**: 159–173.

Stevenson JA, McGarvie DW, Smellie JL, Gilbert JS. 2006. Subglacial and ice-contact volcanism at the Öræfajökull stratovolcano, Iceland. *Bulletin of Volcanology* **68**: 737–752.

Sun SS, McDonough WF., 1989. Chemical and isotopic systems of oceanic basalts: implications for mantle composition and processes. In *Magmatism in Ocean Basins*, Saunders AD, Norry MJ, (eds). *Geological Society of London Special Publication* **42**: 313–345.

Svensson A Andersen KK Bigler M Clausen HB Dahl-Jensen D Davies SM Johnsen SJ Muscheler R Parrenin F Rasmussen SO Röthlisberger R Seierstad I Steffensen JP Vinther BM 2008 A 60 000 year Greenland stratigraphic ice core chronology *Climate of the Past* **4**: 47–57.

Turney CSM. 1998. Extraction of rhyolitic ash from minerogenic lake sediments. *Journal of Paleolimnology* **19**: 199–206.

Walker A, Burgess R, McGarvie D, Smellie J. 2010. Rhyolite volcanism at Öræfajökull Volcano, Iceland – geochemistry, field relations and $^{40}Ar/^{39}Ar$ geochronology. *Geophysical Research Abstracts* **12**: EGU2010-606.

Wastegård S, Björck S, Greve C, Rasmussen TL. 2005. A tephra-based correlation between the Faroe Islands and the Norwegian Sea raises questions about chronological relationships during the last interglacial. *Terra Nova* **17**: 7–12.

Wastegård S, Rasmussen TL. 2001. New tephra horizons from Oxygen Isotope 5 in the North Atlantic: correlation potential for terrestrial, marine and ice-core archives. *Quaternary Science Reviews* **20**: 1587–1593.

Wolff EW, Chappellaz J, Blunier T, Rasmussen SO, Svensson A. 2010. Millennial-scale variability during the last glacial: Tthe ice core record. *Quaternary Science Reviews* **29**: 2828–2838.